Biosynthesis of Silver Nanoparticles from *Achillea Tenuifolia* Aqueous Flower Extract and Its Application for the Efficient Removal of Acid Red 18 and Methyl Orange from Aqueous Media: Isotherm and Kinetics Studies

Yari, Ali; Yari, Mohammad*[*+]

Department of Chemistry, College of Science, Islamshahr Branch, Islamic Azad University, Islamshahr, I.R. IRAN

Sedaghat, Sajjad

Department of Chemistry, College of Science, Shahr-e-Qods Branch, Islamic Azad University, Shahr-e-Qods, I.R. IRAN

Delbari, Sadat Akram

Department of Chemistry, College of Science, Islamshahr Branch, Islamic Azad University, Islamshahr, I.R. IRAN

ABSTRACT: *In this study, the ability of Achillea tenuifolia aqueous flower extract was studied to synthesize silver nanoparticles (AgNPs) for the removal of Acid Red 18 (AR18) and Methyl Orange (MO) from aqueous media. UV-Vis spectroscopy, Scanning Electron Microscopy (SEM), energy-dispersive X-ray (EDX), Transmission Electron Microscopy (TEM), Fourier Transform InfraRed (FT-IR), spectroscopy and X-Ray Diffraction (XRD) analysis were used for the characterization of the prepared AgNPs. The effect of different experimental factors, including pH (3-12), adsorbent dosage (0.1-0.9 g), contact time (5-35 min), and initial concentration of dye (30-50 mg/L) was surveyed. Approximately 94% removal of dye was obtained at a pH of 3 for AR18 and 8 for MO, an adsorbent dosage of 0.9 g, a contact time of 25, and an initial concentration of 30 mg/L. The experimental data were better described by the Langmuir isotherm with the coefficient of determination (R^2) of 0.9998 and 0.9995 for AR18 and MO, respectively. The maximum adsorption capacity (q_{max}) of 112.35 mg/g and 90.90 mg/g was obtained for AR18 and MO, respectively. The kinetic study revealed that the system fitted well with the pseudo-second-order kinetic model (R^2=0.9992 for AR18, R^2=0.9962 for MO). The results of this study demonstrated that synthesized adsorbent is low-cost and eco-friendly, which can be powerfully used for the removal of AR18 and MO dyes from wastewater.*

KEYWORDS: *Green synthesis; Silver nanoparticles; Achillea tenuifolia; Acid red 18; Methyl orange; Isotherm and kinetics studies.*

*****To whom correspondence should be addressed.*

+ *E-mail: ari.mohammad55@yahoo.com*

1021-9986/2023/10/3208-3223 16/$/6.06

INTRODUCTION

Water contamination and its relevant difficulties have already attracted a lot of interest. Today, trying to eliminate this pollutant has become a priority. The development of various industries followed by sewage production has caused many problems in water sources. Synthetic dyes are used in various industries such as plastic, paper, textile, leather, pharmaceuticals, food, and cosmetics, which leads to the production of colored wastewater [1]. Among the types of dyes, azo dyes have a wide variety of structures and easy manufacturing, which has made them more widely used [2].

Acid Red 18 (AR18) (Scheme 1a) is known as a sulfonated azo dye with azo functional groups and aromatic ring structures. It is an anionic food coloring. Also, the wide application of this dye is in the textile industry. Its side effects can include Attention Deficit Hyperactivity Disorder (ADHD) in children, neurobehavioral effects, and reproductive disorders [3-5]. The other azo dye is methyl orange (MO) (Scheme 1b) as an anionic dye. MO is extensively utilized in pharmaceutical, food, paper, printing, and textile industries, as well as research laboratories [6]. MO is considered a serious threat to the environment, animals and human health because its biodegradability is low and the mono-azo group is present in its structure. Excessive exposure to this dye can cause vomiting, diarrhea and even death [7,8]. In addition, the discharge of colored wastewater into the aquatic environment prevents sunlight from entering the water and causes damage to aquatic life [9]. According to the mentioned cases, it is important to remove these dyes before discharge into the environment.

Different techniques such as photocatalysis–ultrafiltration [10], coagulation-flocculation [11], electrocoagulation [12], ozone-electrolysis [13], electrochemistry [14], and photocatalytic oxidation [15-17] have been applied to eliminate AR18 and MO from aqueous solutions. High costs of operation and keeping, the requirement of high energy, the use of chemicals, and even the production of other chemicals are drawbacks of these methods [18]. Compared to the mentioned methods, the adsorption approach is considered to be the most promising and powerful method for the treatment of aqueous media with high efficiency and low-cost. The simplicity of implementation, ease of design, fast process, and potential for the removal of dyes at low concentrations are the other advantages of this method [19-22]. The choice of the adsorbent for the treatment of a dye in wastewater is significant because about 70% of the adsorption operating costs are related to adsorption operations [23].

In recent years, a wide range of essential uses of nanoparticles (NPs) has been reported in the elimination of pollutants. NPs possess a higher surface-to-volume ratio or a greater surface area per weight than larger particles, which has made them more reactive. Silver nanoparticles (AgNPs) as noble metal NPs have received more attention owing to their unique characteristics, such as high surface to volume ratio, great optical property, catalytic activity, electrical conductivity, good oxidative, and high antibacterial activity [24,25]. The chemical reduction route has been applied to synthesize AgNPs with several reductants, including borohydride, sodium citrate, potassium bitartrate, and so on, which are harmful to the environment. The use of toxic solvents such as polyvinyl pyrrolidone and the production of toxic by-products is the other limitations of this way [26,27]. Therefore, natural resources as the reducing agent have gained much attention for the formation of AgNPs. Green synthesis possesses several advantages compared to conventional physicochemical techniques. In particular, it represents a fast, cost-effective, clean, non-toxic, and environmentally friendly method for the synthesis of metal NPs with a wide range of sizes, shapes, compositions, and physicochemical properties [28]. In the green synthesis of NPs, a reducing agent without the usage of any dangerous chemicals such as plants, algae, fungi, microorganisms, biopolymers etc., can be used. Among them, plant extracts are considered as the best option to fabricate AgNPs due to their easiness, cost-effectiveness, access to a wide array of plant resources, and dispersivity of prepared NPs in water. The plant extract comprises phytochemicals such as flavonoids, terpenoids, phenolic compounds, enzymes, and protein, which possess an essential role as a reducing and capping agent [29-31].

Achillea tenuifolia Lam (AT) belongs to the *Asteraceae* family, which is found in the western and northern regions of Iran. The presence of terpenoids and flavonoids has been identified in AT. There are anti-inflammatory, anti-tumor, anti-oxidant, and anti-microbial attributes in AT extract. It is also used as a cough reliever, anti fever, antispasmodic, diuretic, menstrual regulator, appetizer, and wound healing agent [32-34].

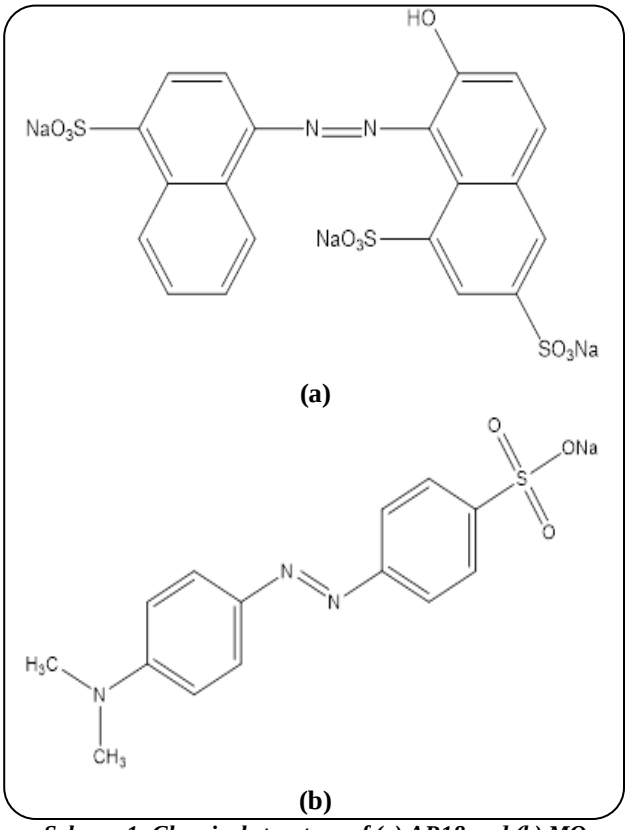

Scheme 1: Chemical structure of (a) AR18 and (b) MO

Abbasi et al., investigated methyl orange organic removal rate on the amount of titanium dioxide nanoparticles in MWCNTs-TiO_2 photocatalyst using statistical methods and Duncan's multiple range test. The photocatalytic results exhibit that the decomposition rate of MO is increased with respect to the weight fraction and illumination time [35]. *Abbasi et al*., used the statistical analysis methodology for the photodegradation of methyl orange using a new nanocomposite containing a modified TiO_2 semiconductor with SnO_2. The variation in the removal efficiency of methyl orange as an organic pollutant with UV irradiation time, weight fraction of synthesised photocatalysts and pH is investigated. The obtained results confirm that the removal efficiency of methyl orange increases in respect of the UV irradiation time and weight fraction [36]. *Abbasi et al.*, represented the investigation of the enhancement and optimization of the photocatalytic activity of modified TiO_2 nanoparticles with SnO_2 nanoparticles using a statistical method. The photocatalytic performance is recorded by variation of the photodecomposition of methyl orange as an organic pollutant with respect to the pH of solution (pH= 3, pH=7 and pH=11), UV irradiation time (ranging from 5 min to 20 min) and weight fraction of photocatalysts (0.1 %wt, 0.2 %wt and 0.3 %wt). According to the obtained results based on Duncan's multiple range test at α=0.05, it can be confirmed that the variations of the removal efficiency with main factors are significant [37].

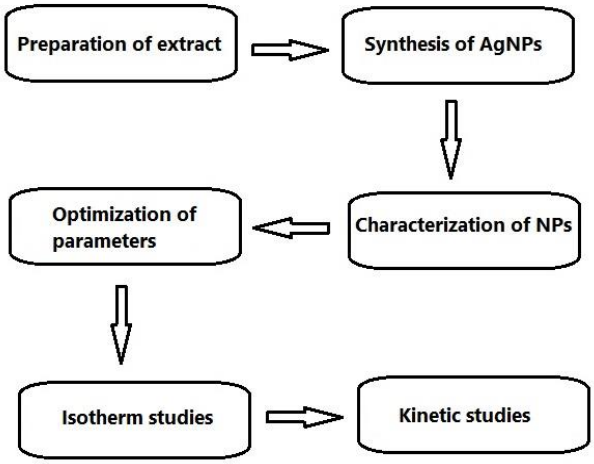

Scheme 2: The steps of the present study

In this study, AgNPs were successfully synthesized by *Achillea tenuifolia* extract to remove the toxic dyes namely AR18 and MO from aqueous solutions. This research focuses on i) estimation of the removal efficiency of AgNPs by investigation of different parameters such as pH, adsorbent dosage, contact time, and initial concentration of dye; ii) describing how the adsorption happened through the analysis of adsorption isotherm models and kinetics; iii) comparing the removal efficiency of AgNPs with other adsorbents for the removal of AR18 and MO (Scheme 2). The aim of this work is to synthesize AgNP using the plant extract, as a low-cost and eco-friendly reducing agent compared to a chemical reducing agent. An absorbent with such advantages is essential for the removal of dyes. To the best of our knowledge, there are no reports for the removal of AR18 and MO using AgNPs synthesized with the *Achillea tenuifolia* extract.

EXPERIMENTAL SECTION

Materials

Silver nitrate ($AgNO_3$) (99.95%), AR18 ($C_{20}H_{11}N_2Na_3O_{10}S_3$), and MO ($C_{14}H_{14}N_3NaO_3S$) were provided from Merck. Flowers of *Achillea tenuifolia* were gathered from Mianeh, East Azerbaijan, Iran, in June 2020.

***Achillea tenuifolia* extract preparation**

First, the fresh flowers of AT was washed by distilled water and these flowers were dried at room temperature. Then, the powdering of plants was accomplished. Afterward, distilled water (100 mL) was added to a certain amount of powder (7 g) and boiling was done at a temperature of 60 ºC for 20 min. The filter paper (Whatman No. 14) was utilized to filter this solution.

Green synthesis of AgNPs

100 mL of 0.01 M $AgNO_3$ solution was prepared. After that, the mixing of this solution with AT extract (10 mL) was performed using mechanical stirring at a rate of 750 rpm with a temperature of 25 ºC for 24 h. The formation of AgNPs is indicated by changing the color of the solution (light brown to dark brown). Then, this solution was centrifuged several times at a rate of 5000 rpm for 20 min. Finally, the drying of AgNPs solution was carried out at a temperature of 70 ºC for 5 h.

Dye removal

In this study, the elimination of AR18 and MO was assessed using fabricated AgNPs via the one-factor-at-a-time (OFAT) method by changing experimental variables such as pH of 3 to 12, contact time of 5 to 35 min, the adsorbent dosage of 0.1 to 0.9 g, and the initial concentration of 30-50 mg/L. The absorption of the samples was recorded using UV–Vis spectrophotometer (Shimadzu double-beam (UV-1800)) at a wavelength of 507 and 464 nm for AR18 and MO, respectively. The removal percentage values were calculated using Eq (1).

$$Removal\ (\%) = \frac{C_0 - C_e}{C_0} \times 100 \qquad (1)$$

Where, the initial concentration of the dye and the final concentration of dye are denoted by C_0 (mg/L) and C_e (mg/L), respectively [38-40].

RESULTS AND DISCUSSION

Effect of different parameters on AgNPs

Effect of extract quantity

The effect of 2, 4, 6, 8, and 10 mL of extract was evaluated on the reaction mixture. It was observed by UV–vis spectra that with the increase of the leaf extract volume to 10 mL, the SPR peak becomes sharper and narrow. Hence, 10 mL was the optimum quantity of leaf extract for the formation of small NPs.

Effect of $AgNO_3$ concentration

The effect of various $AgNO_3$ concentrations (0.01 to 0.05 M) was investigated on the formation of AgNPs. From the SPR peaks obtained, it is clear that at 0.01 M of $AgNO_3$ concentration, the seed formation of silver takes part in the NPs synthesis.

Effect of time

Based on the SPR peaks by UV–vis spectroscopy, it can be observed that peak sharpness increases with the increased time (from 10 to 30 min). The reaction was complete in 30 min and after that, increasing the reaction time has no further effect on the formation of the NPs.

Characterization of the green synthesized AgNPs

Naked-eye observation and UV-Vis analysis

Fig 1 (a) exhibits the reduction of silver ions into AgNPs by a color change from light brown to dark brown. Furthermore, Fig 1 (b) shows the UV-Vis peaks related to the extract alone and different concentrations of $AgNO_3$ along with the extract. The UV–Vis spectrum of *Achillea tenuifolia* extract displays a sharp absorption peak at 315 nm and this wavelength was shifted to 437 nm by the formation of AgNPs. This arises owing to the surface plasmon resonance (SPR) implying combined vibration of electrons corresponding to the metallic AgNPs in resonance with the light waves [41]. It can be concluded that *Achillea tenuifolia* extract could act as a reducing agent in the green synthesis of AgNPs.

SEM and EDX analysis

A Zeiss sigma 500 VP SEM was utilized to survey the surface morphology of the prepared AgNPs. SEM images reveal that the AgNPs have a spherical morphology (Fig 2a). The agglomeration of NPs might be due to the existence of organic molecules, which act as coating agent [30].

The EDX spectrum (Fig 2b) represents the strong element peak with a weight percentage of 68.68%, which is related to silver (Ag). Also, two other peaks are assigned to carbon (C) and chlorine (Cl) with values of 15.72% and 15.61%, respectively. The presence of Ag and Cl in the EDX spectrum reveals that the synthesized NPs contain silver and silver chloride. The existence of C in the EDX spectrum indicated the C=C, C-N, and C-Cl groups in the structure of NPs, which confirms with FT-IR spectrum.

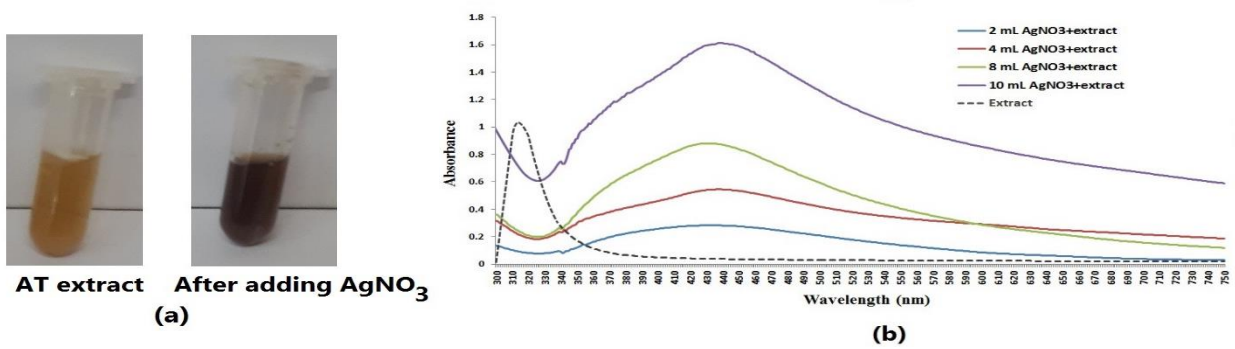

Fig 1: (a) The image of the changing color of the reaction mixture before and after adding $AgNO_3$ and (b) UV-Vis spectra of the green synthesis AgNPs with different concentration of $AgNO_3$

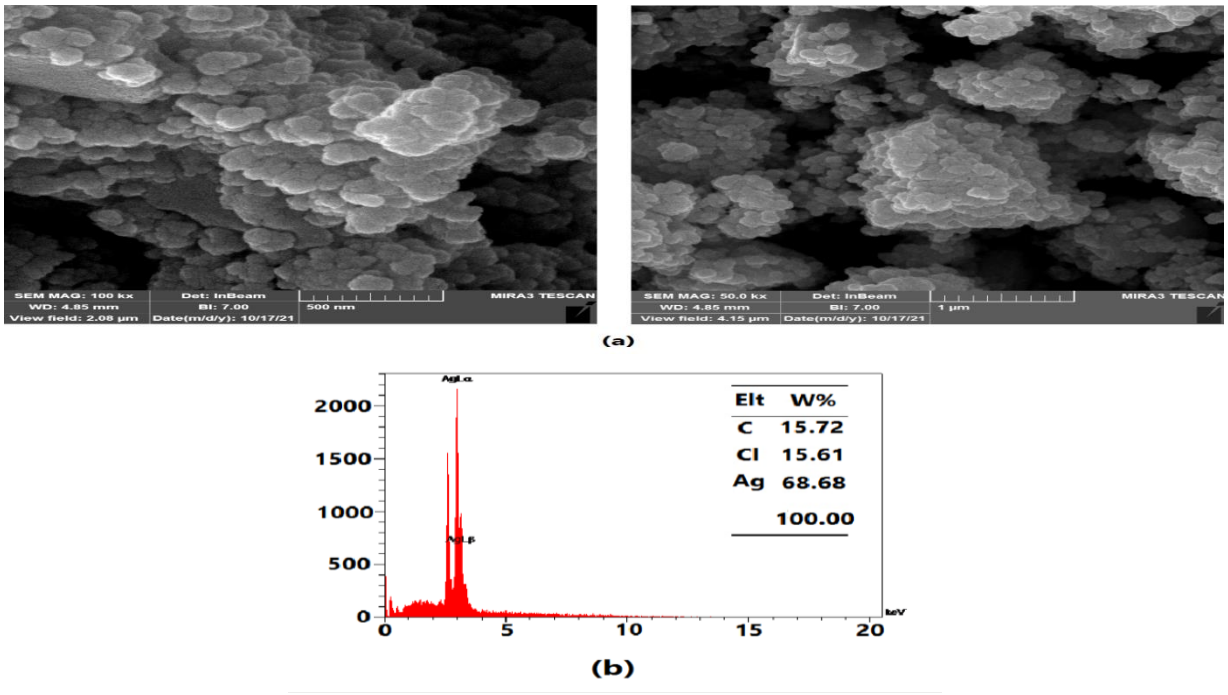

Fig 2: (a) SEM image and (b) EDX spectrum of the synthesized AgNPs

TEM analysis

The morphological property and size of AgNPs were explored by Zeiss TEM 10C-1000Kv (Germany). The average size of particles was found to be 9.70 nm with spherical shape (Fig 3a). This spherical shape of AgNPs is fitted well with the result achieved from the SEM analysis. The AgNPs possess aggregation at certain locations. The size distribution histogram of Dynamic Light Scattering (DLS) confirmed that the size of AgNPs is around 10 nm (Fig 3b).

FT-IR analysis

The determination of the functional groups in the extract of *Achillea tenuifolia* and synthesized AgNPs was done using PerkinElmer Spectrum 100 FT-IR (U.S.A) spectrophotometer by KBr pellet (Fig 4). The absorption peaks at 3414 cm^{-1} and 3436 cm^{-1} are assigned to the OH stretching vibration [42]. The peak at 2379 cm^{-1} was shifted to 2344 cm^{-1}, which is attributed to the C-N group [43]. The band at 1624 cm^{-1} in *Achillea tenuifolia* extract is related to the existence of amide I vibrations. This band was shifted to 1598 cm^{-1} in AgNPs due to the presence of the proteins that possibly are bound to AgNPs via the amine groups [44]. The observed peaks at 1404 cm^{-1} for the extract and at 1358 cm^{-1} for the AgNPs corresponds to the C=C group of alkenes [43]. The C-N stretch of aliphatic amine is presented at 1072 cm^{-1} [45]. Absorption

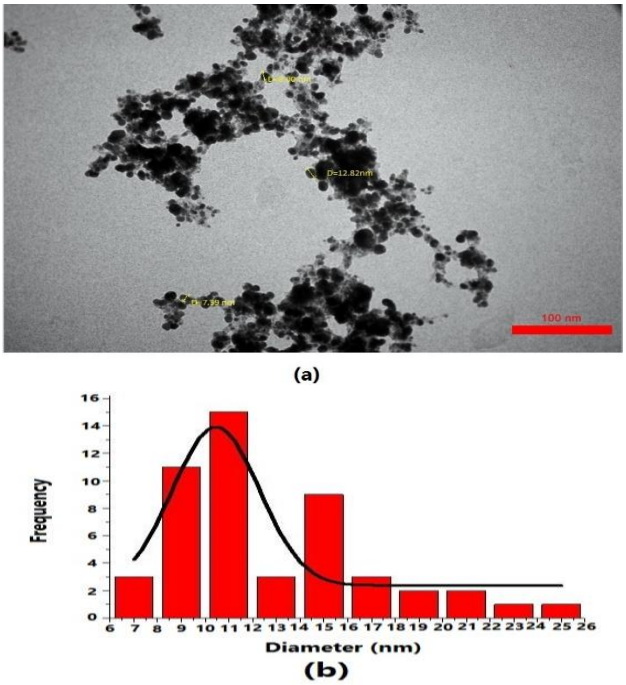

Fig 3: (a) TEM image and (b) histogram with size distribution of the synthesized AgNPs

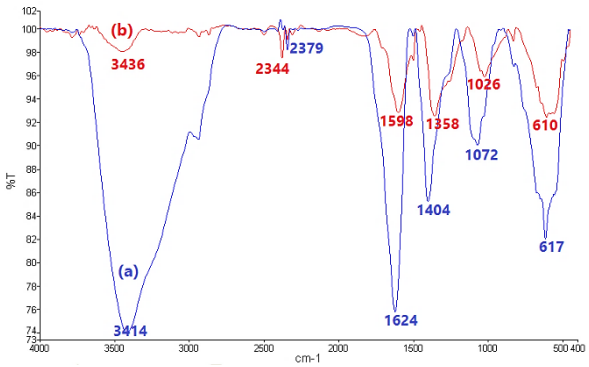

Fig 4: FT-IR spectra of (a) Achillea tenuifolia water extract and (b) AgNPs synthesized using Achillea tenuifolia water extract

peaks at 617 cm^{-1} and 610 cm^{-1} are assigned to the presence of C–Cl. Most of the absorption bands that appeared in the FT-IR spectrum of the *Achillea tenuifolia* extract could also be seen in the FT-IR spectra of AgNPs with a slight displacement.

XRD analysis

The crystalline nature of AgNPs was studied by the Malvern Panalytical X-ray diffractometer (Fig 5). The peaks of silver at 2θ around 38°, 44°, 65°, and 77° are related to the (111), (200), (220), and (311) sets of lattice planes of the face-centered cubic (FCC) structure of silver

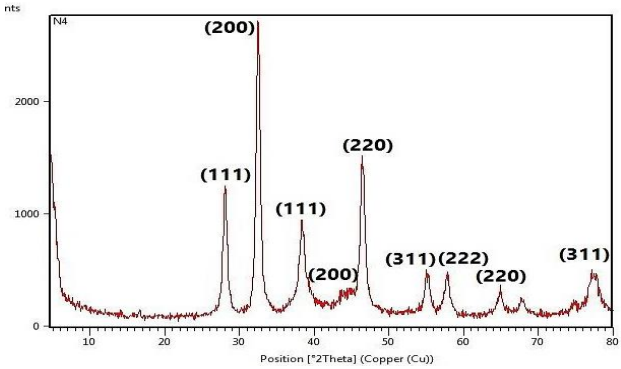

Fig 5. XRD pattern of synthesized AgNPs

and its crystalline nature [46]. Moreover, the other peaks were found at 2θ almost equal to 28°, 32°, 46°, 55°, and 57°, which are assigned to (111), (200), (220), (311), and (222) FCC planes of silver chloride, respectively [47]. The source of chloride ions may be the extract of *Achillea tenuifolia*. Owing to the interaction between Ag ions and Cl ions present in the extract, AgCl NPs are formed. The comparison was performed between the XRD patterns in this study and the pure crystalline silver and silver chloride structure present in Joint Committee on Powder Diffraction Standards (JCPDS) file, which corresponds to no. 04-0783, and 31-1238, respectively [48,49]. A similar observation was reported by *Devi et al.*, for Ag@AgCl NPs synthesized from the leaf extract of Momordica charantia [50]. Also, *Patil et al.*, developed the synthesis of Ag-AgCl NPs using leaf extract of Sasa borealis and the present study results are in good agreement with the present study [51]. The determination of crystallite size was calculated by the Debye–Scherrer's equation (Eq 2).

$$D = \frac{K\lambda}{\beta cos\theta} \qquad (2)$$

Where the average size of the crystals is shown by *D*; *K* is a constant value corresponding to the crystallite structure equal to 0.9; λ (0.154 nm) denotes the wavelength; the peak width and the diffraction angle are demonstrated by β and θ, respectively [52]. The crystallite size was found to be 11 nm, which was close to the particle size of histograms.

Optimization of experimental parameters

Effect of pH

The pH is a key factor in dye adsorption owing to its influence on the adsorbent features and the adsorbate ionization. The degree of ionization of the dye and the mechanism

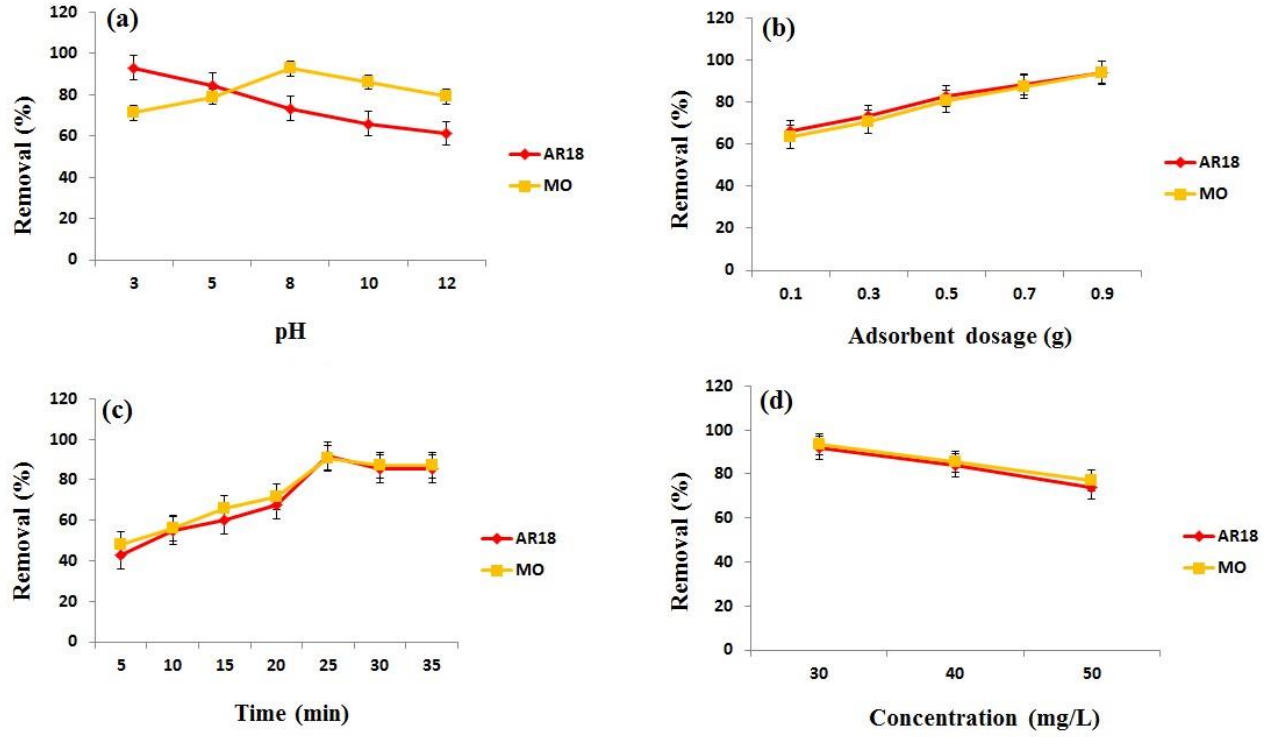

Fig 6: The effect of (a) pH, (b) adsorbent dosage, (c) contact time, and (d) initial concentration of dye for the removal of AR18 and MO

of interaction between the adsorbent with the dye and the ionic charge of the functional groups is affected by pH [2]. Variable pH and other parameters, including adsorbent dosage (0.9 g), initial concentration (30 mg/L), and contact time (25 min) were considered constant. At acidic pHs, the removal percentage of AR18 is high (Fig 6a), which is due to the electrostatic adsorption between the positive charge present on the surface of the AgNPs and negative charge on the AR18 molecules. On the other hand, the number of positive charges on the AgNPs was decreased at higher pHs. Indeed, a competition was created between hydroxyl and the AR18 molecules. Therefore, the removal efficiency was diminished [53]. The maximum removal efficiency (93.14%) of AR18 was observed at pH=3. In the case of MO, has been clearly indicated that the removal efficiency at a pH of 8 is higher than that of other pHs (Fig 6a). It can be attributed to the surface charge of nanoparticles [54-56]. When $pH<pH_{ZPC}$, the adsorbent surface is positively charged, but the surface is negatively charged when $pH>pH_{ZPC}$. The pH_{ZPC} of AgNPs was obtained at 5.11 (Fig 7). The adsorbent surface is covered by positive charges at pH values below 5.11. So, the anionic specie of AR18 is electrostatically attracted by the positive charge of the adsorbent, and the removal percentage of AR18 was increased at a pH of 3.

Effect of adsorbent dosage

The capacity of an adsorbent for a certain initial concentration of the adsorbate (30 mg/L) and pH (3 for AR18 and 8 for MO) is determined by adsorbent dosage. The relationship between the adsorbent dosage and removal percentage of dyes is shown in Fig 6 (b). By increasing the adsorbent dosage, the adsorption sites available for AgNPs–dye interaction were enhanced, whereas the decline in the amount of adsorbate adsorbed per unit mass of adsorbent was owing to adsorption sites remaining unsaturated during the adsorption process [57]. Hence, the adsorbent dosage of 0.9 g shows the maximum removal efficiency for AR18 (94.21%) and MO (93.80%).

Effect of contact time

The adsorption of AR18 and MO by AgNPs in the time range between 5 to 35 min, constant initial concentration of 30 mg/L and pH (3 for AR18 and 8 for MO) is illustrated in Fig 6 (c). The results indicated that the sorption was rapid from 5 min to 25 min, then reach equilibrium at 30 min. This

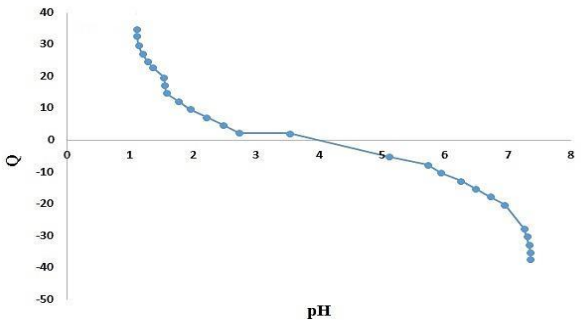

Fig 7: pHZPC curve of AgNPs

behavior is owing to a large number of vacant sites available on the adsorbent surface during the initial stage. In the later stages of contact time, the number of active sites was reduced, which is attributed to the repulsive forces amongst the dye molecules on the solid and bulk phases. On the other hand, by increasing contact time above 25 min, the diffusion becomes more complex because the empty volume within the adsorbent diminishes. So, the tendency of the adsorbent for the adsorption of dye molecules was decreased [58]. *Roozban et al.*, evaluated the different UV irradiation times (5-30 min) for the photodegradation of MO. The higher degradation was observed at 30 min [59]. Abbasi indicated that the enhancement of irradiation time from 5 to 35 min led to a remarkable increase in MO degradation [60].

Effect of initial concentration

Fig 6 (d) shows the influence of initial concentration on the percentage removal of AR18 and MO at constant pH (3 for AR18 and 8 for MO), contact time (25 min), and adsorbent dosage (0.9 g). The removal efficiency was reduced with the increment in the initial concentration of both dyes. This may be owing to the fewer number of available active sites on the surface of the adsorbent for the high concentration of AR18 and MO. At lower concentrations of dye, the adsorbent surface was still unsaturated at equilibrium and more sites were occupied by dye molecules at higher concentrations due to the concentration gradient [61].

Adsorption isotherm

The data were described by the two most widely used adsorption isotherm models named Langmuir and Freundlich. Based on the Langmuir model, sorption is a monolayer process. It is assumed that there are a limited number of adsorption sites on the surface of the adsorbent. When a dye molecule occupies an adsorption site, no further sorption can happen at that location for the reason that the most molecule of adsorbate it can hold is one. The linear expression of this model is shown in Eq (3).

$$\frac{C_e}{q_e} = \frac{1}{q_m K_L} + \frac{1}{q_m} C_e \qquad (3)$$

Where the concentration of adsorbate in the solution at the equilibrium state is denoted by C_e (mg/L), q_e is the adsorption capacity at the equilibrium state (mg/g), q_m (mg/g) is the maximum monolayer adsorption capacity related to the adsorbent, and the affinity of adsorbate to the adsorbent is described by K_L (L/mg) as Langmuir constant. C_e/q_e versus Ce chart is applied to calculate q_m and K_L from the slope and intercept of the straight line, respectively (Fig 8a). When the empirical data fit well with the Langmuir model, a dimensionless constant separation factor (R_L) can be expressed (Eq 4).

$$R_L = \frac{1}{1 + K_L C_0} \qquad (4)$$

Where C_0 (mg/L) displays the maximum initial dye concentration. The R_L parameter represents the adsorption nature. $R_L = 0$, $0 < R_L < 1$, $R_L = 1$, and $R_L > 1$ indicated irreversible, favorable, linear, and unfavorable adsorption, respectively [62]. R_L values for the AR18 and MO were found to be 0.604 and 0.279, respectively. These results indicate favorable monolayer adsorption.

In the Freundlich model, it is assumed that the surface is heterogeneous, and various analytes are adsorbed as multilayer adsorption [63]. The Freundlich isotherm model can be described as a linear form (Eq 5).

$$Log\ q_e = log\ (K_F) + \frac{1}{n}\ log\ (C_e) \qquad (5)$$

K_F is a constant value of the sorption intensity, and 1/n is corresponding to the nature of adsorption. The K_F and 1/n values can be determined by measuring the slope and intercept from the plot of Log q_e versus Log C_e (Fig 8b) [63,64]. It can be said that the uptake is favorable, unfavorable, and irreversible if $0 < 1/n < 1$, $1/n > 1$, and $1/n = 1$, respectively [65]. In this investigation, the 1/n values were obtained at 0.7542 and 0.3758 for AR18 and MO, respectively, indicating the favorability of adsorption.

The data obtained in the present study revealed a better fit with the Langmuir model with a coefficient of determination (R^2) equal to 0.9998 and 0.9995 for the adsorption of AR18 and MO, respectively (Fig 7). The obtained parameters related to the mentioned isotherm models are summarized in Table 1.

Table 1: The obtained parameters of isotherm models for the removal of AR18 and MO

Isotherms	Parameters	AR18	MO
Langmuir	q_{max} (mg/g)	112.35	90.90
	K_L (L/mg)	0.0218	0.0860
	R^2	0.9998	0.9995
	R_L	0.6045	0.2793
Freundlich	K_f (mg/g)	3.441	18.531
	1/n	0.7542	0.3758
	R^2	0.9839	0.9589

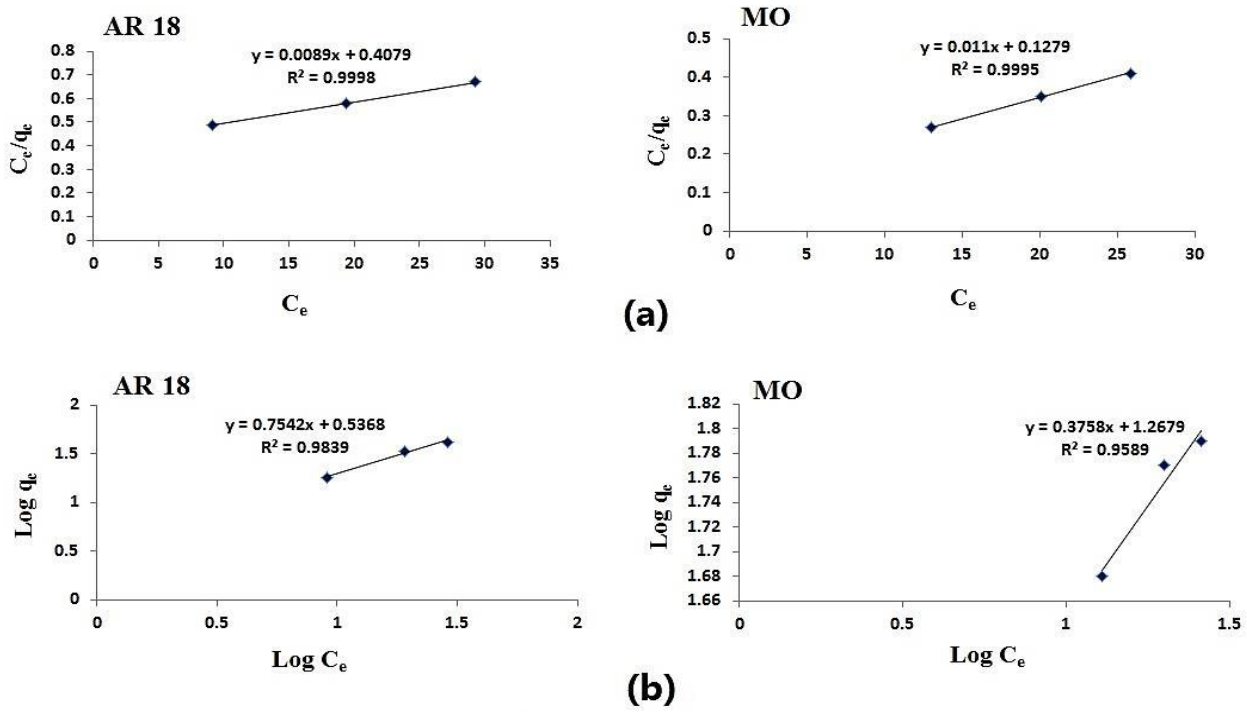

Fig 8: (a) Langmuir and (b) Freundlich isotherms for the removal of AR18 and MO by synthesized AgNPs

Adsorption kinetics

In order to specify the influence of contact time on feasible mechanisms during the removal process, adsorption kinetics were evaluated [66]. In this study, pseudo-first-order (PFO) and pseudo-second-order (PSO) models were used.

The PFO and PSO models can be expressed through Eqs (6) and (7).

$$ln\,(q_e - q_t) = lnq_e - k_1(t) \quad (6)$$

$$\frac{t}{q_t} = \frac{1}{k_2 q_e^2} + \frac{t}{q_e} \quad (7)$$

Herein q_e and q_t (mg/g) demonstrated the capacity of ions adsorbed at equilibrium and time *t*. Also, K_1 (min^{-1}) and K_2 (g/mg.min) are the constant rates of PFO and the constant rate of PSO, respectively. The plot of ln (q_e-q_t) against (t) was used to determine (q_e) and (K_1) in the first model (Fig 9a), whereas the plot of (q_t/t) vs. (t) was utilized to calculate the (q_e) and (K_2) factors in the second model (Fig 9b) [67]. The values of the R^2 related to the PSO model were 0.9992 and 0.9962 for AR18 and MO, respectively, while in the PFO model, the values of R^2 were 0.9511 and 0.9597 for AR18 and MO, respectively. This implies that the adsorption of both dyes follows the PSO model. Hence, chemisorption was considered as a major role in the adsorption process of AR18 and MO [68]. The calculated factors, including K_1, K_2, q_e, and R^2 are listed in Table 2.

Using adsorbent to real sample (Textile effluent)

The real effluent was provided by the dyeing unit of the textile factory. The aim of this study was to assess the efficiency of the adsorbent in reducing pollution. The efficiency

Table 2: The obtained kinetic parameters for the removal of AR18 and MO

Kinetic	Parameters	AR18	MO
Pseudo-first-order	K_1 (min^{-1})	0.0616	0.0705
	q_e (mg/g)	16.94	22.19
	R^2	0.9511	0.9597
Pseudo-second-order	K_2 ($g.mg^{-1}. Min^{-1}$)	6.47×10^{-3}	3.91×10^{-3}
	q_e (mg/g)	28.73	29.76
	R^2	0.9992	0.9962

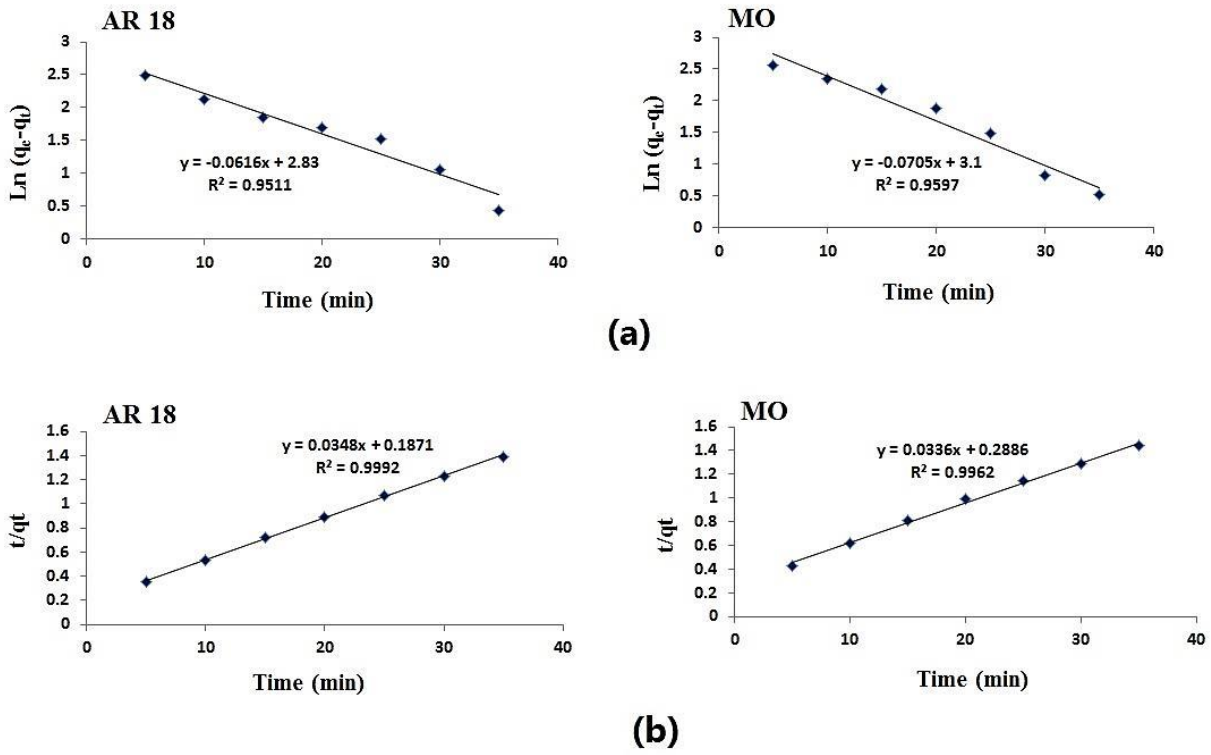

Fig 9: (a) Pseudo first-order and (b) Pseudo second-order adsorption kinetics of adsorption process for AR18 and MO

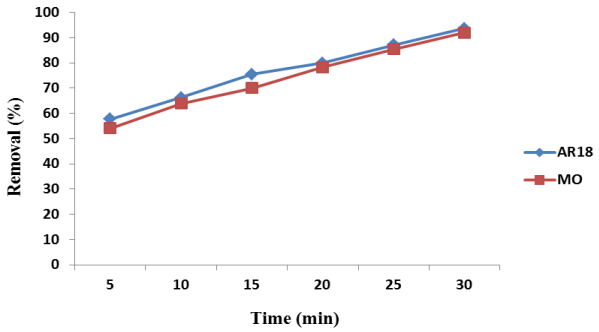

Fig 10: Effect of adsorbent to real sample (textile effluent) at various times

of the adsorbent on the real sample was studied after 30 min and by adding 1 g of adsorbent. The amount of residual dye was determined by spectrophotometer and the removal efficiency was calculated. The removal efficiency was found to be 93.65% and 92% for AR18 and MO, respectively (Fig 10). This adsorbent is suitable as a low-cost and eco-friendly adsorbent for the removal of dyes from wastewater.

Selectivity study

The high adsorption capability of synthesized adsorbent towards AR18 and MO dyes has also been surveyed compared to other azo dyes (Ponceau 4R (P-4R) and Acid red 88 (AR88)). The selectivity study of AgNPs was examined using fixed concentrations (30 mg/L) of different dye solutions. Fig 11 exhibits the removal percentage

Table 3: Comparison of adsorption capacities of various adsorbents for AR18, MO, and other dyed

Adsorbent	Type of dye	q_{max} (mg/g)	Removal efficiency (%)	Time (min)	Ref.
GFH[1]	AR18	29.13	78.59	85	[1]
Activated charcoal	AR18	10.75	90.83	60	[2]
Moringa peregrina ash	MO	15.43	96.00	70	[6]
Cs/Tn/MMT[2]	MO	57.37	95.62	30	[7]
Populous leaves	MO	90.44	---	45	[8]
OLPAC[3]	MO	33.00	96.00	40	[9]
AgNPs using *Salvinia molesta*	MB	121.04	---	60	[24]
AgNPs using *Zanthoxylum armatum*	MB	---	---	1440	[42]
Polyaniline/HCl-MRH[4]	AR18	100.00	>90.00	120	[69]
AgNPs using *Thespesia populnea* bark	MB	---	92.00	120	[70]
AgNPs	AR18	112.35	>94.00	25	Present study
AgNPs	MO	90.90	>93.00	25	Present study

[1] Granular Ferric Hydroxide (GFH)
[2] Chitosan/tannin/montmorillonite
[3] Orange and lemon peels-derived activated carbon
[4] Polyaniline/HCl-modified rice husk

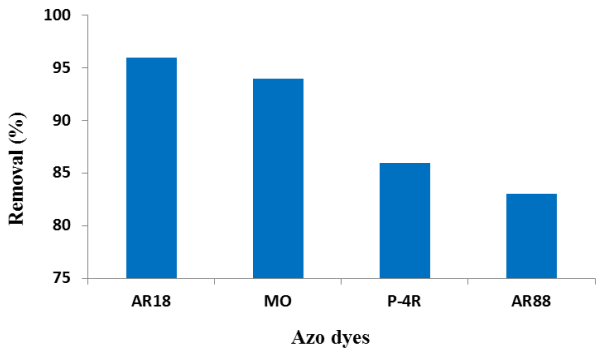

Fig 11: The elimination rate of different dyes by AgNPs

of different dyes adsorbed by AgNPs. The results revealed that the removal percentage of AR18, MO, P-4R, and AR 88 was 96%, 94%, 86%, and 83%, respectively. Hence, this adsorbent suggests the high adsorption selectivity towards azo dyes.

Comparative study

The maximum adsorption capacity (q_{max}), removal efficiency, type of dye, and contact time of AgNPs along with other adsorbents reported in previous articles for the adsorption of AR18 and MO are presented in Table 3. Three adsorbents namely *Moringa peregrina* ash, chitosan/tannin/montmorillonite, as well as orange and lemon peels-derived activated carbon reveals the removal efficiency of 96%, 95.62%, and 96% with a contact time of 70 min, 30 min, and 40 min, respectively. These contact times are higher than the contact time of AgNPs. The q_{max} values of all adsorbents are lower than q_{max} of AgNPs for the AR18 (112.35 mg/g) and MO (90.90 mg/g). Compared to other adsorbents available in Table 3, the synthesized AgNPs in the present study possess a higher q_{max} and removal percentage with less contact time.

CONCLUSIONS

In this study, a simple, fast, environmentally friendly, and low-cost approach for the synthesis of AgNPs using the *Achillea tenuifolia* extract was developed to remove AR18 and MO from aqueous solutions. The characterization of synthesized AgNPs was performed using UV–Vis spectrophotometry, SEM, EDX, TEM, FT-IR, and XRD. The parameters affecting the removal efficiency such as pH, adsorbent dosage, contact time, and initial concentration of dye were optimized. pH was 3 and 8 for AR18 and MO, respectively. The adsorbent dosage of 0.9 g, contact time of 25, and initial concentration of 30 mg/L were obtained for both dyes. In order to describe the adsorption process, adsorption isotherm and kinetic models were implemented. Langmuir isotherm and pseudo-second-order kinetic showed the best fit to the experimental data with R^2 value of 0.9998 and 0.9992, respectively. Overall, the synthesized AgNPs using the green procedure indicated excellent performance for the elimination of AR18 and MO, which can extensively be utilized in the treatment of dye sewage from different industries without any special conditions.

Received :Dec.15, 2022 ; Accepted : Apr. 17, 2023

REFERENCES

[1] Hamidi F., Dehghani M. H., Kasraee M., Salari M., Shiri L., Mahvi A. H., Acid Red 18 Removal from Aqueous Solution by Nanocrystalline Granular Ferric Hydroxide (GFH); Optimization by Response Surface Methodology & Genetic-Algorithm, *Scientific Reports*, **12:** 4761 (2022).

[2] Najafi Chaleshtori, A., Mohammadi Meghadddam, A., Sadeghi, M.M., Rahimi, R.R., Hemati, S., Ahmadi, A., Removal of Acid Red 18 (Azo-Dye) from Aqueous Solution by Adsorption onto Activated Charcoal Prepared from Almond Shell, *Journal of Environmental Science and Management*, **20:** 9-16 (2017).

[3] Mohammadi H., Ghaedi M., Fazeli M., Sabzehmeidani M.M., Removal of Hexavalent Chromium Ions and Acid Red 18 by Superparamagnetic $CoFe_2O_4$/Polyaniline Nanocomposites Under External Ultrasonic Fields, *Microporous and Mesoporous Materials*, **324**: 111275 (2021).

[4] Malakootian, M., Mahdizadeh, H., Khavari, M., Nasiri, A., Amiri Gharaghani, M., Khatami, M., Sahle-Demessie, E., Varma, R. S., Efficiency of Novel Fe/Charcoal/Ultrasonic Micro-electrolysis Strategy in the Removal of Acid Red 18 from Aqueous Solutions, *Journal of Environmental Chemical Engineering*, **8**: 103553 (2020).

[5] Chen, Y., Long, W., Xu, H., Efficient removal of Acid Red 18 from aqueous Solution by in-Situ Polymerization of Polypyrrole-Chitosan Composites, *Journal of Molecular Liquids*, **287**: 110888 (2019).

[6] Bazrafshan E., Allah Zarei A., Nadi H., Zazouli M.A., Adsorptive Removal of Methyl Orange and Reactive Red 198 dyes by Moringa Peregrina Ash, *Indian Journal of Chemical Technology*, **21**: 105-113 (2014).

[7] Tahari N., De Hoyos-Martinez P. L., Izaguirre N., Houwaida N., Abderrabba M., Ayadi S., Labidi J., Preparation of Chitosan/tannin and Montmorillonite Films as Adsorbents for Methyl Orange Dye Removal, *International Journal of Biological Macromolecules*, **210**: 94–106 (2022).

[8] Shah S.S., Sharma T., Dar B.A., Bamezai R.K., Adsorptive Removal of Methyl Orange dye from Aqueous Solution Using Populous Leaves: Insights from Kinetics, Thermodynamics and Computational Studies, *Environmental Chemistry and Ecotoxicology*, **3**: 172–181 (2021).

[9] Ramutshatsha-Makhwedzha D., Mavhungu A., Lucey Moropeng M., Mbaya R., Activated Carbon Derived from Waste Orange and Lemon Peels for the Adsorption of Methyl Orange and Methylene Blue Dyes from Wastewater, *Heliyon*, **8**: e09930 (2022).

[10] Mozia S., Tomaszewska M., Morawski A.W., Removal of Azo-Dye Acid Red 18 in Two Hybrid Membrane Systems Employing a Photodegradation Process, Desalination. **198**: 183–190 (2006).

[11] Ben Dassi R., Chamam B., Trabelsi I., Combination of Coagulation-Flocculation and Adsorption on Granular Activated Carbon for Color Removal from AR18 and Real Textile Wastewater, *Journal of the Tunisian Chemical Society*, **19**: 295-302 (2017).

[12] Irki S., Ghernaout, D., Wahib Naceur M., Alghamdi A., Aichouni M., Decolorizing Methyl Orange by Fe-Electrocoagulation Process– A Mechanistic Insight, *International Journal of Environmental Chemistry*, **2**: 18-28 (2018).

[13] Basiri Parsa J., Golmirzaei M., Abbasi M., Degradation of Azo dye C.I. Acid Red 18 in Aqueous Solution by Ozone-Electrolysis Process, *Journal of Industrial and Engineering Chemistry*, **20**: 689-694 (2014).

[14] Yousefi Z., Zafarzadeh A., Mohammadpour R. A., Zarei E., Mengelizadeh N., Ghezel A., Electrochemical Removal of Acid Red 18 Dye from Synthetic Wastewater Using a Three-Dimensional Electrochemical Reactor, *Desalination and Water Treatment*, **165**: 352–361 (2019).

[15] Abbasi S., Adsorption of Dye Organic Pollutant Using Magnetic ZnO Embedded on the Surface of Graphene Oxide, *Journal of Inorganic and Organometallic Polymers and Materials*, **30**: 1924–1934 (2020).

[16] Abbasi S., Ahmadpoor F., Imani M., Ekrami-Kakhki M.S., Synthesis of Magnetic Fe_3O_4@ZnO@Graphene Oxide Nanocomposite for Photodegradation of Organic Dye Pollutant, *International Journal of Environmental Analytical Chemistry*, **100**: 225-240 (2020).

[17] Abbasi S., Response Surface Methodology for Photo Degradation of Methyl Orange Using Magnetic Nanocomposites Containing Zinc Oxide, *Journal of Cluster Science*, **32**: 805–812 (2021).

[18] Arum Sari A., Amriani F., Intan Satria Akhmad R., Rylo Pambudi M., Putra Pamungkas R., Muryanto M., Adsorption of Acid Red and Acid Orange with Adsorbent from Bioethanol Black Liquor Sludge, *AIP Conference Proceedings*, **2024**: 020007 (2018).

[19] Dawodu F. A., Onuh C. U., Akpomie K.G., Unuabonah E. I., Synthesis of Silver Nanoparticle from Vigna Unguiculata Stem as Adsorbent for Malachite Green in a Batch System, *SN Applied Sciences*, **1**: 346 (2019).

[20] Ediati R., Aulia W., Nikmatin B.A., Hidayat A.R.P., Fitriana U.M., Muarifah C., Sulistiono D.O., Martak F., Prasetyoko D., Chitosan/UiO-66 Composites as High-Performance Adsorbents for the Removal of Methyl Orange in Aqueous Solution, *Materials Today Chemistry*, **21**: 100533 (2021).

[21] Mehmandost N., Goudarzi N., Arab Chamjangali M., Bagherian Gh., Application of Chemometrics Tools for Removal of Crystal Violet and Methylene Blue in Binary Solution by Eco-Friendly Magnetic Adsorbent Modified on Heracleum Persicum Waste, *Spectrochimica Acta Part A: Molecular and Biomolecular Spectroscopy*, **292**: 122415 (2023).

[22] Ashrafi Ghadamali Bagherian M., Arab Chamjangali M., Goudarzi N., Removal of Brilliant Green and Crystal violet from Mono- and Bi-component Aqueous Solutions Using NaOH-modified Walnut Shell, *Analytical and Bioanalytical Chemistry Research*, **1**: 95-114 (2018).

[23] Mehmandost N., Goudarzi N., Arab Chamjangali M., Bagherian Gh., Application of Random forest for Modeling Batch and Continuous Fixed-Bed Removal of Crystal Violet from Aqueous Solutions Using Gypsophila Aretioides Stem-Based Biosorbent, *Spectrochimica Acta Part A: Molecular and Biomolecular Spectroscopy*. **265**: 120292 (2022).

[24] Batool M., Daoush W.M., Khalid Hussain M., Dye Sequestration Using Biosynthesized Silver Nanoparticles Adsorbent in Aqueous Solutions, *Crystals*. **12**: 662 (2022).

[25] Khodadadi B., Bordbar M., Nasrollahzadeh M., Achillea Millefolium L. Extract Mediated Green Synthesis of Waste Peach Kernel Shell Supported Silver Nanoparticles: Application of the Nanoparticles for Catalytic Reduction of a Variety of Dyes in Water, *Journal of Colloid and Interface Science*, **493**: 85-93 (2017).

[26] Roy A., Bulut O., Some S., Kumar Mandal A., Deniz Yilmaz M., Green Synthesis of Silver Nanoparticles: Biomolecule-Nanoparticle Organizations Targeting Antimicrobial Activity, *RSC Advances*, **9**: 2673–2702 (2019).

[27] Isa N., Lockman Z., Methylene Blue Dye Removal on Silver Nanoparticles Reduced by Kyllinga Brevifolia, *Environmental Science and Pollution Research*, **26**: 11482–11495 (2019).

[28] Bahrulolum H., Nooraei S., Javanshir N., Tarrahimofrad H., Mirbagheri V.S., Easton A.J., Ahmadian G., Green Synthesis of Metal Nanoparticles Using Microorganisms and their Application in the Agrifood Sector, *Journal of Nanobiotechnology*, **19**: 86 (2021).

[29] Khwannimit D., Maungchang R., Rattanakit P., Green synthesis of Silver Nanoparticles Using Clitoria Ternatea Flower: An Efficient Catalyst for Removal of Methyl Orange, *International Journal of Environmental Analytical Chemistry*, **102**: 5247-5263 (2022).

[30] Khare S., Kumar Singh R., Prakash O., Green Synthesis, Characterization and Biocompatibility Evaluation of Silver Nanoparticles Using Radish Seeds, *Results in Chemistry*, **4**: 100447 (2022).

[31] Elhawary,S., EL-Hefnawy H., Alzahraa Mokhtar F., Sobeh M., Mostafa E., Osman S., El-Raey M., Green Synthesis of Silver Nanoparticles Using Extract of Jasminum officinal L. Leaves and Evaluation of Cytotoxic Activity Towards Bladder (5637) and Breast Cancer (MCF-7) Cell Lines, *International Journal of Nanomedicine*, **15**: 9771–9781 (2020).

[32] Rabbi Angourani H., Phytochemical Compounds of Achillea Tenuifolia Lam Essential oil in Zanjan Province Natural Habitats, *Journal of Medicinal Plants Biotechnology*, **5**: 8-12 (2019).

[33] Bagheri Y., Fathi E., Maghoul A., Moshtagh S., Mokhtari K., Abdollahpour A., Montazersaheb S., Bagheri A., Effects of Achillea tenuifolia Lam. Hydro-Alcoholic Extract on Anxiety-Like Behavior and Reproductive Parameters in Rat Model of Chronic Restraint Stress, *Human and Experimental Toxicology*, **40**: 1852-1866 (2021).

[34] Aminkhani A., Sharifi R., Dorosti R., Chemical Composition and Antimicrobial Activity of Achillea Tenuifolia Lam. Essential oil at Different Phenological Stages from Khoy, *Chemistry & Biodiversity*, **16**: e1900289 (2019).

[35] Abbasi S., Dastan D., Ţălu S., Tahir,M.B., Elias M., Tao L., Li Z., Evaluation of the Dependence of Methyl Orange Organic Pollutant Removal Rate on the Amount of Titanium Dioxide Nanoparticles in MWCNTs-TiO2 Photocatalyst Using Statistical Methods and Duncan's Multiple Range Test, *International Journal of Environmental Analytical Chemistry*, (2022).

[36] Abbasi S., Hasanpour M., Ahmadpoor F., Sillanpää M., Dastan D., Achour A., Application of the Statistical Analysis Methodology for Photodegradation of Methyl Orange Using a New Nanocomposite Containing Modified TiO_2 Semiconductor with SnO_2, *International Journal of Environmental Analytical Chemistry*, **101**: 208-224 (2021).

[37] Abbasi S., Investigation of the Enhancement and Optimization of the Photocatalytic Activity of Modified TiO_2 Nanoparticles with SnO_2 Nanoparticles Using Statistical Method, *Materials Research Express*, **5**: 6 (2018).

[38] Dawood S., Kanti Sen T., Phan C., Adsorption Removal of Methylene Blue (MB) dye from Aqueous Solution by Bio-Char Prepared from Eucalyptus Sheathiana Bark: Kinetic, Equilibrium, Mechanism, Thermodynamic and Process Design, *Desalination and Water Treatment*, **57**: 28964-28980 (2016).

[39] Roozban N., Abbasi S., Ghazizadeh M., Statistical Analysis of the Photocatalytic Activity of Decorated Multi-Walled Carbon Nanotubes with ZnO Nanoparticles, *Journal of Materials Science: Materials in Electronics*, **28**: 6047–6055 (2017).

[40] Abbasi S., Photocatalytic Activity Study of Coated Anatase-Rutile Titania Nanoparticles with Nanocrystalline Tin Dioxide Based on the Statistical Analysis, *Environmental Monitoring and Assessment*, **191**: 206 (2019).

[41] Venkatesan J., Kim, S.K., Shim M.S., Antimicrobial, Antioxidant, and Anticancer Activities of Biosynthesized Silver Nanoparticles Using Marine Algae Ecklonia Cava, *Nanomaterials*, **6**: 235 (2016).

[42] Jyoti K., Singh A., Green Synthesis of Nanostructured Silver Particles and Their Catalytic Application in Dye Degradation, *Journal of Genetic Engineering and Biotechnology*, **14**: 311–317 (2016).

[43] Azizi M., Sedaghat S., Tahvildari K., Derakhshi P., Ghaemi A., Synthesis of Silver Nanoparticles Using Peganum Harmala Extract as a Green Route, *Green Chemistry Letters and Reviews*, **10**: 420–427 (2017).

[44] Prakash P., Gnanaprakasam P., Emmanuel R., Arokiyaraj S., Saravanan M., Green Synthesis of Silver Nanoparticles from Leaf Extract of Mimusops Elengi, Linn. for Enhanced Antibacterial Activity Against Multi Drug Resistant Clinical Isolates, *Colloids and Surfaces B: Biointerfaces*, **108**: 255–259 (2013).

[45] Wadia Alshameri A., Owais M., Altaf I., Farheen S., Rumex Nervosus Mediated Green Synthesis of Silver Nanoparticles and Evaluation of its in Vitro Antibacterial, and Cytotoxic Activity, *OpenNano*, **8**: 100084 (2022).

[46] Li J., Ma Q., Shao H., Zhou X., Xia H., Xie J., Biosynthesis, Characterization, and Antibacterial Activity of Silver Nanoparticles Produced from Rice Straw Biomass, *BioResource*, **12**: 4897-4911 (2017).

[47] Al Aboody M.S., Silver/Silver Chloride (Ag/AgCl) Nanoparticles Synthesized from Azadirachta Indica Lalex and its Antibiofilm Activity Against Fluconazole Resistant Candida Tropicalis, *Artificial Cells, Nanomedicine, and Biotechnology*, **47**: 2107–2113 (2019).

[48] Prakash Patil M., Dheerendra Singh R., Bhimrao Koli P., Tumadu Patil K., Sonu Jagdale B., Rajesh Tipare A., Kim G. D., Antibacterial Potential of Silver nanoparticles Synthesized Using Madhuca Longifolia Flower Extract as a Green Resource, *Microbial Pathogenesis*, **121**: 184-189 (2018).

[49] Venkatesan J., Kim S. K., Suk Shim M., Antimicrobial, Antioxidant, and Anticancer Activities of Biosynthesized Silver Nanoparticles Using Marine Algae Ecklonia Cava, *Nanomaterials*, **6**: 235 (2016).

[50] Devi T.B., Ahmaruzzaman Begum S., A Rapid, Facile and Green Synthesis of Ag@AgCl Nanoparticles for the Effective Reduction of 2, 4-Dinitrophenyl Hydrazine, *New Journal of Chemistry*, **40**: 1497-1506 (2016).

[51] Prakash Patil M., Palma,J., Chantal Simeon N., Jin X., Liu X., Ngabire D., Kim N.H., Hiralal Tarte N., Kim G.D., Sasa Borealis Leaf Extract-Mediated Green Synthesis of Silver-Silver Chloride Nanoparticles and Their Antibacterial and Anticancer Activities, *New Journal of Chemistry*, **41**: 1363-1371 (2017).

[52] Nasseh N., Sadat Arghavan F., Daglioglu N., Asadi A., Fabrication of Novel Magnetic $CuS/Fe_3O_4/GO$ Nanocomposite for Organic Pollutant Degradation under Visible Light Irradiation, *Environmental Science and Pollution Research*, **28**: 19222–19233 (2021).

[53] Zhang W.X., Lai L., Mei P., Li Y., Li Y.H., Liu Y., Enhanced Removal Efficiency of Acid Red 18 from Aqueous Solution Using Wheat Bran Modified by Multiple Quaternary Ammonium Salts, *Chemical Physics Letters*, **710**: 193–201 (2018).

[54] Altaf Nazir M., Aswad Bashir M., Najam T., Sufyan Javed M., Suleman S., Hussain Sh., Parkash Kumar O., Shoai Ahmad Shah S., Rehman A., Combining Structurally Ordered Intermetallic Nodes: Kinetic and Isothermal Studies for Removal of Malachite Green and Methyl Orange with Mechanistic Aspects, *Microchemical Journal*, **164**: 105973 (2021).

[55] Abbasi S., Hasanpour M., The Effect of pH on the Photocatalytic Degradation of Methyl Orange Using Decorated ZnO Nanoparticles with SnO_2 Nanoparticles, *Journal of Materials Science: Materials in Electronics*, **28**: 1307–1314 (2017).

[56] Abbasi S., Hasanpour M., Variation of the Photocatalytic Performance of Decorated MWCNTs (MWCNTs-ZnO) with pH for Photo Degradation of Methyl Orange, *Journal of Materials Science: Materials in Electronics*, **28**: 11846–11855 (2017).

[57] Jiang R., Fu Y. Q., Zhu H. Y., Yao J., Xiao L., Removal of Methyl Orange from Aqueous Solutions by Magnetic Maghemite/Chitosan Nanocomposite Films: Adsorption Kinetics and Equilibrium, *Journal of Applied Polymer Science*, **125**: E540-E549 (2012).

[58] El Gamal M., Mohamed F.M., Mekewi M.A., Hashem F.S., El-Aassard M.R., Khalifa R.E., Adsorptive Removal of Methyl Orange from Aqueous Solutions by Polyvinylidene Fluoride Tri-Flouro Ethylene/Carbon Nanotube/Kaolin Nanocomposite: Kinetics, Isotherm, and Thermodynamics, *Desalination and Water Treatment*, **193**: 142–151 (2020).

[59] Roozban N., Abbasi S., Ghazizadeh M., The Experimental and Statistical Investigation of the Photo Degradation of Methyl Orange Using Modified MWCNTs with Different Amount of ZnO Nanoparticles, *Journal of Materials Science: Materials in Electronics*, **28**: 7343–7352 (2017).

[60] Abbasi S., The Degradation Rate Study of Methyl Orange Using $MWCNTs@TiO_2$ as Photocatalyst, Application of Statistical Analysis Based on Fisher's F Distribution, *Journal of Cluster Science*, **33**: 593–602 (2022).

[61] Pal J., Kanti Deb M., Kumar Deshmukh D., Verma D., Removal of Methyl Orange by Activated Carbon Modified by Silver Nanoparticles, *Applied Water Science*, **3**: 367–374 (2013).

[62] Sterenzon E., Kumar Vadivel V., Gerchman Y., Luxbacher T., Narayanan R., Mamane H., Effective Removal of Acid Dye in Synthetic and Silk Dyeing Effluent: Isotherm and Kinetic Studies, *ACS Omega*, **7**: 118−128 (2022).

[63] Alswieleh A.M., Efficient Removal of Dyes from Aqueous Solution by Adsorption on L-Arginine-Modified Mesoporous Silica Nanoparticles, Processes, **10**: 1079 (2022).

[64] Taher T., Antini R., Indwi Saputri L., Rahma Dian A., Said M., Lesbani A., Removal of Congo Red and Rhodamine B Dyes from Aqueous Solution by Raw Sarolangun Bentonite: Kinetics, Equilibrium and Thermodynamic Studies, *AIP Conference Proceedings*, **2049**: 020011 (2018).

[65] Saxena M., Sharma N., Saxena R., Highly Efficient and Rapid Removal of a Toxic Dye: Adsorption Kinetics, Isotherm, and Mechanism Studies on Functionalized Multiwalled Carbon Nanotubes, *Surfaces and Interfaces*, **21**: 100639 (2020).

[66] Villabona-Ortíz Á., Figueroa-Lopez K. J., Ortega-Toro R., Kinetics and Adsorption Equilibrium in the Removal of Azo-Anionic Dyes by Modified Cellulose, *Sustainability*, **14**: 3640 (2022).

[67] Fawaz Mutar R., Anhab Saleh M., Optimization of Arsenic Ions Adsorption and Removal from Hospitals Wastewater by Nano-Bentonite Using Central Composite Design, *Materials Today: Proceedings*, **60**: 1248-1256 (2022).

[68] Yousefi M., Gholami,M., Oskoei V., Mohammadi A. A., Baziar M., Esrafili A., Comparison of LSSVM and RSM in Simulating the Removal of Ciprofloxacin from Aqueous Solutions Using Magnetization of Functionalized Multi-Walled Carbon Nanotubes: Process Optimization Using GA and RSM Techniques, *Journal of Environmental Chemical Engineering*, **9**: 105677 (2021).

[69] Shabandokht M., Binaeian E., Tayebi,H. A., Adsorption of Food dye Acid red 18 Onto Polyaniline-Modified Rice Husk Composite: Isotherm and Kinetic Analysis, *Desalination and Water Treatment*, **57**: 27638-27650 (2016).

[70] Tahir M.Y., Ahmad A., Alothman A.A., Saleh Mushab M.S., Ali S., Green Synthesis of Silver Nanoparticles Using Thespesia populnea Bark Extract for Efficient Removal of Methylene Blue (MB) Degradation via Photocatalysis with Antimicrobial Activity and for Anticancer Activity, *Bioinorganic Chemistry and Applications*, **3**: 1-12 (2022).